Inorganic Chemistry
Article

Inorg. Chem. **2009**, *48*, 10281–10288 **10281**
DOI: 10.1021/ic901409y

Trinuclear Terpyridine Frustrated Spin System with a $Mn^{IV}_3O_4$ Core: Synthesis, Physical Characterization, and Quantum Chemical Modeling of Its Magnetic Properties

Carole Baffert,[†,¶] Maylis Orio,[‡,§] Dimitrios A. Pantazis,[‡,§] Carole Duboc,*[,†] Allan G. Blackman,[∥] Geneviève Blondin,[⊥] Frank Neese,[‡,§] Alain Deronzier,[†] and Marie-Noëlle Collomb*[,†]

[†]*Université Joseph Fourier Grenoble 1/CNRS, Département de Chimie Moléculaire, UMR-5250, Laboratoire de Chimie Inorganique Redox, Institut de Chimie Moléculaire de Grenoble FR- CNRS-2607, BP-53, 38041 Grenoble Cedex 9, France,* [‡]*Institut für Physikalische und Theoretische Chemie, University of Bonn, Wegelerstrasse 12, 53115 Bonn, Germany,* [§]*Max-Planck-Institut für Bioanorganische Chemie, Stiftstrasse 34-36, D-45470 Mülheim an der Ruhr, Germany,* [∥]*Department of Chemistry, University of Otago, P.O. Box 56, Dunedin, New Zealand, and* [⊥]*Institut de Recherches en Technologies et Sciences pour le Vivant (iRTSV), Laboratoire de Chimie et Biologie des Métaux (LCBM), Physico-chimie des Métaux en Biologie (PMB), UMR 5249, CNRS-CEA-UJF, 17 Avenue des Martyrs, F-38054 Grenoble Cedex 9, France.* [¶]*Current address: Laboratoire de Bioénergétique et Ingénierie des Protéines, UPR 9036, Université de Provence et CNRS, 13402 Marseille Cedex 20, France.*

Received July 18, 2009

The trinuclear oxo bridged manganese cluster, $[Mn^{IV}_3O_4(terpy)(terpyO_2)_2(H_2O)](S_2O_8)_2$ (**5**) (terpy = 2,2′:2″,6′-terpyridine and $terpyO_2$ = 2,2′:2″,6′-terpyridine 1,1″-dioxide), was isolated in an acidic aqueous medium from the reaction of $MnSO_4$, terpy, and oxone as chemical oxidant. The $terpyO_2$ ligands were generated in situ during the synthesis by partial oxidation of terpy. The complex crystallizes in the monoclinic space group $P2_1/n$ with a = 14.251(5) Å, b = 15.245(5) Å, c = 24.672(5) Å, α = 90.000(5)°, β = 92.045(5)°, γ = 90.000(5)°, and Z = 4. The triangular $\{Mn^{IV}_3O_4\}^{4+}$ core observed in this complex is built up of a basal $Mn(\mu\text{-}O)_2Mn$ unit where each Mn ion is linked to an apical Mn ion via mono(μ-O) bridges. The facial coordination of the two tridentate $terpyO_2$ ligands to the $Mn(\mu\text{-}O)_2Mn$ unit allows the formation of the triangular core. **5** is also the first structurally characterized Mn complex with polypyridinyl N-oxide ligands. The variable-temperature magnetic susceptibility data for this complex, in the range of 10−300 K, are consistent with an S = 1/2 ground state and were fit using the spin Hamiltonian $H_{eff} = -2J_a(\hat{S}_1\hat{S}_2+\hat{S}_1\hat{S}_3) - 2J_b\hat{S}_2\hat{S}_3$ with $S_1 = S_2 = S_3 = 3/2$, J_a = −37 (±0.5) and J_b = −53 (±1) cm^{-1}, where J_a and J_b are exchange constants through the mono-μ-oxo and the di-μ-oxo bridges, respectively. The doublet ground spin state of **5** is confirmed by EPR spectroscopic measurements. Density functional theory (DFT) calculations based on the broken symmetry approach reproduce the magnetic properties of **5** very well (calculated values: J_a = −39.4 and J_b = −55.9 cm^{-1}), thus confirming the capability of this quantum chemical method for predicting the magnetic behavior of clusters involving more than two metal ions. The nature of the ground spin state of the magnetic $\{Mn^{IV}_3O_4\}^{4+}$ core and the role of ancillary ligands on the magnitude of J are also discussed.

Introduction

Oxo-bridged manganese clusters have attracted significant interest because of their remarkable magnetic properties resulting from the exchange interaction between paramagnetic Mn centers[1,2] and their relevance to biological systems.[3−8] Hundreds of complexes with varying core topology and nuclearity have been isolated in the past decades. Frequently, the complexes involve carboxylate ligands.

*To whom correspondence should be addressed. E-mail: marie-noelle.collomb@ujf-grenoble.fr (M.-N.C.), carole.duboc@ujf-grenoble.fr (C.D.).

(1) Sessoli, R.; Gatteschi, D.; Caneschi, A.; Novak, M. A. *Nature* **1993**, *365*, 141–143.
(2) Bagai, R.; Christou, G. *Chem. Soc. Rev.* **2009**, *38*, 1011–1026.
(3) Weatherburn, D. C.; Mandal, S.; Mukhopadhyay, S.; Bahduri, S.; Lindoy, L. F. Manganese. In *Comprehensive Coordination Chemistry II*; McCleverty, J. A., Meyer, T. J., Eds.; Elsevier Pergamon: Oxford, 2004; Vol. *5*, p 1.
(4) Mukhopadhyay, S.; Mandal, S. K.; Bhaduri, S.; Armstrong, W. H. *Chem. Rev.* **2004**, *104*, 3981–4026.
(5) Wu, A. J.; Penner-Hahn, J. E.; Pecoraro, V. L. *Chem. Rev.* **2004**, *104*, 903–938.
(6) Mullins, C. S.; Pecoraro, V. L. *Coord. Chem. Rev.* **2008**, *252*, 416–443.
(7) Cady, C. W.; Crabtree, R. H.; Brudvig, G. W. *Coord. Chem. Rev.* **2008**, *252*, 444–455.
(8) Collomb, M.-N.; Deronzier, A. *Eur. J. Inorg. Chem.* **2009**, 2025–2046.

Published on Web 10/01/2009

Concomitant with the structural variability a wide range of magnetic properties are observed. In fact, understanding the key structural and electronic factors that control the exchange interactions between the metal centers is one of the key motivations for the synthesis of the target systems.

The trinuclear compounds with oxo bridges reported to date[4,6,9] can be divided into four structural core types: the oxo-centered $\{Mn_3(\mu_3\text{-}O)\}^{6+/7+}$ (i), the adamantane-shaped $\{Mn^{IV}{}_3(\mu\text{-}O)_3(\mu_3\text{-}XO_4)\}^{3+}$ (ii) $\{Mn^{IV}(\mu\text{-}O)_2Mn^{IV}\text{-}(\mu\text{-}O)_2Mn^{IV}\}^{4+}$ (iii) and the triangular $\{Mn^{IV}{}_3O_4\}^{4+}$ (iv) (Scheme 1).

The μ_3-O clusters, also referred to as "basic carboxylates" (type (i)), are the most intensely studied systems.[10,11] A large number of compounds isolated in both homo $Mn^{III}{}_3$ and mixed valence $Mn^{II}Mn^{III}{}_2$ have been reported. On the other hand, types (ii) and (iii) are only represented by the $[Mn_3(\mu\text{-}O)_3(tacn)_3(\mu_3\text{-}XO_4)]^{3+}$,[12] (tacn = 1,4,7-triazacyclononane) and $[Mn_3O_4(O_2CCH_3)_4(bpy)_2]$[13] (bpy = 2,2′-bipyridine) complexes, respectively. The clusters of type (iv) that have been reported to date are limited to the following four systems: $[Mn_3O_4(bpy)_4(Cl)_2]MnCl_4$ (**1**),[14] $[Mn_3O_4(bpy)_4(OH_2)_2](ClO_4)_4$ (**2**),[15] $[Mn_3O_4(phen)_4(OH_2)_2](NO_3)_4$ (**3**),[16] and $[Mn_3O_4(bpea)_3(OH)](ClO_4)_3$ (**4**),[17] in which the ancillary ligands are *N*-based bidentate (phen = 1,10-phenanthroline) or tridentate (bpea = *N,N*-bis(2-pyridylmethyl)ethylamine)). This core is also found in the hexanuclear $[\{Mn^{IV}{}_3(\mu\text{-}O)_4(OH)(tpen)\}_2(\mu\text{-}tpen)](ClO_4)_6$ compound, which consists of two $\{Mn^{IV}{}_3O_4\}^{4+}$ units linked by one tpen moiety (tpen = *N*, *N*,*N*′,*N*′-tetrakis(2-pyridylmethyl)-1,2-ethanediamine).[18] In our ongoing synthetic exploration of manganese complexes with the tridentate 2,2′:6′,2″-terpyridine ligand (terpy),[19−26] we have isolated the trinuclear $[Mn^{IV}{}_3O_4(terpy)(terpyO_2)_2(H_2O)]^{4+}$ (**5**) complex ($terpyO_2$ = 2,2′:6′,2″-terpyridine 1,1″-dioxide), which provides another example of this triangular core. We report here the synthesis and the structural characterization of this complex. Although the terpy ligand has been successfully used for the synthesis of several dinuclear[19,20,27,28] and linear tetranuclear[29−31] oxo-bridged Mn complexes, its meridional coordination mode has so far prevented the isolation of this peculiar $\{Mn^{IV}{}_3\text{-}(\mu\text{-}O)_4\}^{4+}$ core. The formation of **5** was achieved owing to the facial coordination of the two $terpyO_2$ ligands, which were in situ generated during the synthesis. This compound is also the first structurally characterized Mn complex with polypyridinyl N-oxide ligands. Prior to this work, only mononuclear Mn^{II} mononuclear complexes have been isolated with such ligands but their X-ray structures were not obtained.[32−34]

Interestingly, the magnetic behavior of the $\{Mn^{IV}{}_3(\mu\text{-}O)_4\}^{4+}$ trinuclear complexes depends on the geometrical features of the core with ground spin states of $S = 1/2$ for **1**[14] and **2**[15] and 3/2 for **4**.[17] In this work, the magnetic properties of **5** are investigated with the help of Electron Paramagnetic Resonance (EPR) spectroscopy and magnetic susceptibility measurements. In addition, to rationalize the ground spin state of this frustrated spin system, broken symmetry (BS) density functional theory (DFT) is relied upon.[35,36] Numerous studies have shown that this is presently the most reliable method for predicting the magnetic exchange interactions in polynuclear complexes of the size and complexity studied here.[37] While the majority of the previous studies have been performed on dinuclear systems,[38] some successful theoretical investigations have been reported on complexes of higher nuclearity,[39−43] as exemplified by our recent work on a tetranuclear Mn cluster in two different oxidation states.[44,45]

Experimental Section

Materials. Manganese(II) sulfate ($MnSO_4\cdot H_2O$, Aldrich), 2,2′:6′,2″-terpyridine (terpy, 99.9%, Alfa Aesar), and oxone ($2KHSO_5\cdot KHSO_4\cdot K_2SO_4$, Aldrich) were used as supplied.

(9) Kessissoglou, D. P. *Coord. Chem. Rev.* **1999**, *186*, 837–858.
(10) Viciano-Chumillas, M.; Tanase, S.; Mutikainen, I.; Turpeinen, U.; de Jongh, L. J.; Reedijk, J. *Inorg. Chem.* **2008**, *47*, 5919–5929.
(11) Cano, J.; Cauchy, T.; Ruiz, E.; Milios, C. J.; Stoumpos, C. C.; Stamatatos, T. C.; Perlepes, S. P.; Christou, G.; Brechin, E. K. *Dalton Trans.* **2008**, 234–240.
(12) Wieghardt, K.; Bossek, U.; Nuber, B.; Weiss, J.; Gehring, S.; Haase, W. *J. Chem. Soc., Chem. Commun.* **1988**, 1145–1146.
(13) Bhaduri, S.; Pink, M.; Christou, G. *Chem. Commun.* **2002**, 2352–2353.
(14) Auger, N.; Girerd, J. J.; Corbella, M.; Gleizes, A.; Zimmermann, J. L. *J. Am. Chem. Soc.* **1990**, *112*, 448–450.
(15) Sarneski, J. E.; Thorp, H. H.; Brudvig, G. W.; Crabtree, R. H.; Schulte, G. K. *J. Am. Chem. Soc.* **1990**, *112*, 7255–7260.
(16) Reddy, K. R.; Rajasekharan, M. V.; Arulsamy, N.; Hodgson, D. J. *Inorg. Chem.* **1996**, *35*, 2283–2286.
(17) Pal, S.; Chan, M. K.; Armstrong, W. H. *J. Am. Chem. Soc.* **1992**, *114*, 6398–6406.
(18) Pal, S.; Armstrong, W. H. *Inorg. Chem.* **1992**, *31*, 5417–5423.
(19) Collomb, M.-N.; Deronzier, A.; Richardot, A.; Pécaut, J. *New J. Chem.* **1999**, *23*, 351–353.
(20) Baffert, C.; Collomb, M.-N.; Deronzier, A.; Pécaut, J.; Limburg, J.; Crabtree, R. H.; Brudvig, G. W. *Inorg. Chem.* **2002**, *41*, 1404–1411.
(21) Mantel, C.; Hassan, A. K.; Pécaut, J.; Deronzier, A.; Collomb, M.-N.; Duboc-Toia, C. *J. Am. Chem. Soc.* **2003**, *125*, 12337–12344.
(22) Mantel, C.; Philouze, C.; Collomb, M.-N.; Duboc, C. *Eur. J. Inorg. Chem.* **2004**, 3880–3886.
(23) Baffert, C.; Romero, I.; Pécaut, J.; Llobet, A; Deronzier, A.; Collomb, M.-N. *Inorg. Chim. Acta* **2004**, *357*, 3430–3436.
(24) Mantel, C.; Baffert, C.; Romero, I.; Deronzier, A.; Pécaut, J.; Collomb, M.-N.; Duboc, C. *Inorg. Chem.* **2004**, *43*, 6455–6463.
(25) Mantel, C.; Chen, H. Y.; Crabtree, R. H.; Brudvig, G. W.; Pécaut, J.; Collomb, M. N.; Duboc, C. *ChemPhysChem* **2005**, *6*, 541–546.
(26) Romain, S.; Duboc, C.; Neese, F.; Rivière, E.; Hanton, L. R.; Blackman, A. G.; Philouze, C.; Leprêtre, J.-C.; Deronzier, A.; Collomb, M.-N. *Chem.—Eur. J.* **2009**, *15*, 980–988.
(27) Limburg, J.; Vrettos, J. S.; Liable-Sands, L. M.; Rheingold, A. L.; Crabtree, R. H.; Brudvig, G. W. *Science* **1999**, *283*, 1524–1527.
(28) Limburg, J.; Vrettos, J. S.; Chen, H. Y.; de Paula, J. C.; Crabtree, R. H.; Brudvig, G. W. *J. Am. Chem. Soc.* **2001**, *123*, 423–430.
(29) Chen, H.; Faller, J. W.; Crabtree, R. H.; Brudvig, G. W. *J. Am. Chem. Soc.* **2004**, *126*, 7345–7349.
(30) Baffert, C.; Romain, S.; Richardot, A.; Leprêtre, J.-C.; Lefebvre, B.; Deronzier, A.; Collomb, M.-N. *J. Am. Chem. Soc.* **2005**, *127*, 13694–13704.
(31) Chen, H. Y.; Collomb, M.-N.; Duboc, C.; Blondin, G.; Rivière, E.; Faller, J. W.; Crabtree, R. H.; Brudvig, G. W. *Inorg. Chem.* **2005**, *44*, 9567–9573.
(32) Reiff, W. M.; Baker, W. A., Jr. *Inorg. Chem.* **1970**, *9*, 570–576.
(33) Morrison, M. M.; Sawyer, D. T. *Inorg. Chem.* **1978**, *17*, 338–339.
(34) Ito, K.; Nagata, T.; Tanaka, K. *Inorg. Chem.* **2001**, *40*, 6331–6333.
(35) Noodleman, L. *J. Chem. Phys.* **1981**, *74*, 5737–5743.
(36) Noodleman, L.; Davidson, E. R. *Chem. Phys.* **1986**, *109*, 131–143.
(37) Neese, F. *Coord. Chem. Rev.* **2009**, *253*, 526–563.
(38) Ruiz, E.; Alvarez, S.; Rodriguez-Fortea, A.; Alemany, P.; Pouillon, Y.; Massobrio, C. In *Molecules to materials*; Miller, J. S., Drillon, M., Eds.; Wiley-VCH: Weinheim, 2001.
(39) Noodleman, L.; Case, D. A. *Adv. Inorg. Chem.* **1992**, *38*, 423–470.
(40) Noodleman, L.; Peng, C. Y.; Case, D. A.; Mouesca, J. M. *Coord. Chem. Rev.* **1995**, *144*, 199–244.
(41) Ruiz, E.; Rodriguez-Fortea, A.; Cano, J.; Alvarez, S.; Alemany, P. *J. Comput. Chem.* **2003**, *24*, 982–989.
(42) Ruiz, E. *Struct. Bonding* (*Berlin*) **2004**, *113*, 91–102.
(43) Shoji, M.; Koizumi, K.; Kitagawa, Y.; Kawakami, T.; Yamanaka, S.; Okumura, M.; Yamaguchi, K. *Chem. Phys. Lett.* **2006**, *432*, 343–347.
(44) Pantazis, D. A.; Orio, M.; Petrenko, T.; Zein, S.; Bill, E.; Lubitz, W.; Messinger, J.; Neese, F. *Chem.—Eur. J.* **2009**, *15*, 5108–5123.
(45) Pantazis, D. A.; Orio, M.; Petrenko, T.; Zein, S.; Lubitz, W.; Messinger, J.; Neese, F. *Phys. Chem. Chem. Phys.* **2009**, *11*, 6788–6798.

Scheme 1. Oxo-Manganese Core Structures of Known Manganese Trinuclear Complexes

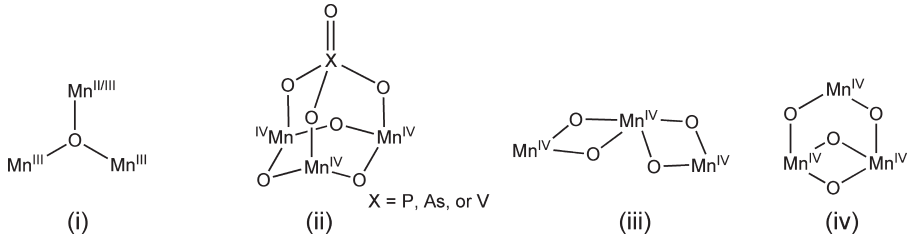

Synthesis of $[Mn_3^{IV}O_4(terpy)(terpyO_2)_2(H_2O)](S_2O_8)_2$ (5). A 10 mM solution of H_2SO_4 in H_2O (pH 2) was prepared by addition of 25.5 μL of H_2SO_4 (18 M) to 50 mL of H_2O. Solid terpy (0.100 g, 0.429 mmol) and oxone (0.111 g, 0.181 mmol) were added to 10 mL of this H_2SO_4 solution. The solution was stirred until dissolution of the solids was complete (about 1 h). A solution of $MnSO_4 \cdot H_2O$ (0.073 g, 0.429 mmol) in 3 mL of H_2SO_4 solution was added to the mixture which turned from yellow to green. Solid oxone (0.111 g, 0,180 mmol) was then added, and the solution turned red-brown. Crystals of $5 \cdot 3.54H_2O$ suitable for X-ray diffraction were obtained by slow evaporation of the solution at room temperature after 2 days. Yield: 40 mg (8%). Anal. Calcd for $C_{45}H_{35}Mn_3O_{25}S_4N_9 \cdot 5H_2O$ (1484.96): C, 36.39; H, 3.05; N, 8.49. Found: C, 36.40; H, 2.84; N, 8.42. Selected IR bands (cm^{-1}): 3428 (m), 3086 (m), 1651 (w), 1633 (w), 1604 (m), 1567 (w), 1498 (w), 1484 (m), 1455 (m), 1434 (m), 1395 (w), 1330 (w), 1282 (vs), 1262 (vs), 1199 (s), 1165 (s), 1096 (m), 1043 (s), 852 (m), 817 (w), 778 (s), 744 (m), 724 (m), 677 (s), 625 (m), 589 (m), 561 (m), 412 (w), 345 (w).

Crystallographic Measurements. Diffraction data were collected on a Bruker SMART diffractometer with Mo Kα radiation, and all calculations were performed using the SHELXTL computer program.[46] A brown monoclinic prism of dimensions $0.2 \times 0.1 \times 0.02$ mm^3 was selected. Full details of the X-ray structure determination and the crystallographic data are available in the Supporting Information, Table S1.

EPR Spectroscopy. The Q-band EPR spectrum was recorded with a Bruker EMX, equipped with the ER-5106 QTW Bruker cavity and an Oxford Instruments ESR-900 continuous-flow helium cryostat for the Q-band experiments at 4.5 K.

Magnetic Susceptibility Measurements. Magnetic susceptibility data were recorded on a MPMS5 magnetometer (Quantum Design Inc.). The calibration was made at 298 K using a palladium reference sample furnished by Quantum Design Inc. The data were collected over the temperature range 10−300 K and were corrected for diamagnetism and for the presence of an impurity of $[Mn(terpy)_2](S_2O_8)$ at a concentration of 0.8% molar in Mn.

Computational Details. All theoretical calculations were based on DFT and have been performed with the ORCA program package.[47] To facilitate comparisons between theory and experiment, we optimized the X-ray structure of the complex while constraining the positions of all heavy atoms to their experimentally derived coordinates. Thus, only the positions of the hydrogen atoms were relaxed since these are not reliably determined from X-ray diffraction. Geometry optimization was performed for the high-spin (HS) state with the GGA functional BP86[48,49] using the TZVP basis set[50] for all atoms and taking advantage of the RI approximation with the auxiliary TZV/J Coulomb fitting basis sets.[51] Increased integration grids (Grid4 in ORCA convention) and tight SCF convergence criteria were used. Single-point Broken-Symmetry DFT calculations were performed with the hybrid meta-GGA functional TPSSh,[52] which was singled out among several functionals as the best performer in our recent benchmark studies.[44,53,54] All alternative spin configurations for the broken-symmetry calculations were generated with the "FlipSpin" feature of ORCA. Final energy levels were computed by direct diagonalization of the Heisenberg Hamiltonian, and the magnetic susceptibility curves were reconstructed from theoretical data with the JulX program.[55]

Results and Discussion

Synthesis. The reaction conditions used to prepare **5** were similar to those employed previously for the synthesis of the $[Mn^{IV}_2O_2(terpy)_2(SO_4)_2]$ complex,[28] except that oxone was first added to the terpy ligand solution before addition of the manganese salt. This procedure leads to the in situ generation of some amount of $terpyO_2$ by partial oxidation of the terpy ligand (formation of N-oxide on the distal nitrogen atoms). The presence of these oxygen atoms increases the flexibility of the ligand and allows its facial coordination as well as the formation of a trinuclear complex with the $\{Mn^{IV}_3(\mu\text{-}O)_4\}^{4+}$ core, readily formed in acidic aqueous conditions. Indeed all trinuclear complexes with this core were isolated under similar acidic conditions.[14−17] Complex **5** is obtained in rather poor yield, and no other complexes such as high-valent μ-oxo polynuclear or low-valent Mn mononuclear complexes crystallized in parallel. Moreover, **5** is insoluble in organic or aqueous solvents, preventing its study in solution.

Crystal Structure of $5 \cdot 3.54H_2O$. The structure consists of the trinuclear cation $[Mn_3^{IV}O_4(terpy)(terpyO_2)_2(H_2O)]^{4+}$, two peroxodisulfate anions, and water molecules included within the lattice. Three Oak Ridge thermal ellipsoid plot (ORTEP) views of the complex are shown in Figure 1, and selected bond distances and angles are listed in Table 1. Table 2 summarizes the average distances and angles of the $\{Mn^{IV}_3O_4\}^{4+}$ core in this complex along with those of complexes **1**−**4**.

The three manganese atoms in **5** occupy the vertices of an isosceles triangle. One of the Mn atoms (Mn(1)) is linked to the other two (Mn(2) and Mn(3)) by a single μ-oxo bridge (O(4) and O(3), respectively). Mn(2) and

(46) Sheldrick, G. M. *SHELXTL-Plus, Structure Determination Software Programs*, version 5.1; Bruker-AXS Inc.: Madison, WI, 1998.
(47) Neese, F. *ORCA - an ab initio, Density Functional and Semiempirical Program Package*, v. 2.6-35; Universität Bonn: Bonn, Germany, 2007.
(48) Becke, A. D. *Phys. Rev. A* **1988**, *38*, 3098–3100.
(49) Perdew, J. P. *Phys. Rev. B* **1986**, *33*, 8822–8824.
(50) Schäfer, A.; Huber, C.; Ahlrichs, R. *J. Chem. Phys.* **1994**, *100*, 5829–5835.
(51) Weigend, F. *Phys. Chem. Chem. Phys.* **2006**, *8*, 1057–1065.
(52) Staroverov, V. N.; Scuseria, G. E.; Tao, J. M.; Perdew, J. P. *J. Chem. Phys.* **2003**, *119*, 12129–12137.
(53) Kossmann, S.; Kirchner, B.; Neese, F. *Mol. Phys.* **2007**, *105*, 2049–2071.
(54) Orio, M.; Pantazis, D. A.; Petrenko, T.; Neese, F. *Inorg. Chem.* **2009**, *48*(15), 7251–7260.
(55) Bill, E. *JulX (v. 1.41), 1.41*; Max-Planck-Institut für Bioanorganische Chemie: Mülheim an der Ruhr, Germany, 2008.

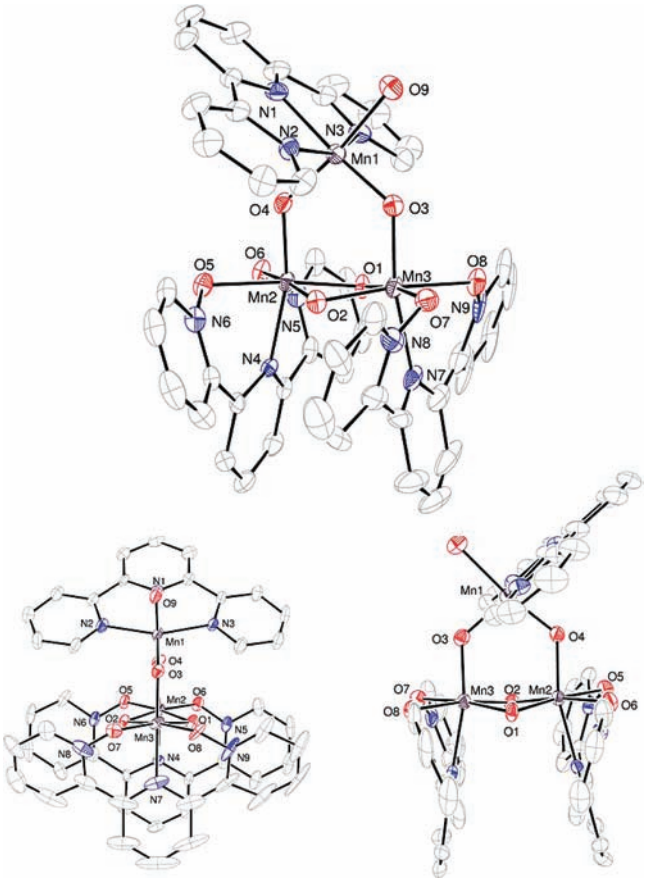

Figure 1. Three ORTEP views of the molecular structure of complex **5**, including the atom labeling scheme.

Mn(3) are linked by a bis-μ-oxo bridge (O(1) and O(2)). The three manganese atoms and the two mono μ-oxo bridges O(3) and O(4) are coplanar, while the O(1) and O(2) atoms of the bis-μ-oxo bridge form a segment perpendicular to this plane. The $Mn_2(\mu\text{-}O)_2$ moiety, is also almost planar (the dihedral angle between the planes (Mn(3), O(1), O(2)) and (Mn(2), O(1), O(2)) is equal to 161.8°). A similar $\{Mn^{IV}{}_3O_4\}^{4+}$ core was also observed in the bpy (**1**[14] and **2**[15]) and phen (**3**[16]) complexes. On the other hand, the hydroxyl-bound bpea complex **4** exhibits a considerable deviation with respect to the plane formed by the three Mn atoms and the two single μ-oxo bridges (the dihedral angle being 26.6°, Table 2), because of hydrogen bonding between the hydroxo group and an oxygen atom of the doubly bridged segment (see below).[17] The Mn(1)−Mn(2), Mn(1)−Mn(3), and Mn(2)−Mn(3) distances (3.2230(18), 3.242(18), 2.6772(17) Å, respectively) are close to those observed in **1**−**3** and longer than those found for **4**. In the basal $Mn_2(\mu\text{-}O)_2$ unit, the Mn−O distances (average 1.8145 Å), the O−Mn−O (average 83.15°) and Mn−O−Mn angles (average 94.64°) are characteristic of this structure. Distances and angles about the apical Mn(1) atom (Mn(1)−O(3), O(4) = 1.761(5) Å and O(3)−Mn(1)−O(4) = 100.1(2)°) are also close to those observed for complexes **1**−**3**. The coordination geometry of each of the manganese atoms in **5** is distorted octahedral. The coordination sphere of Mn(1) consists of three nitrogen atoms of the terpy ligand and three oxygen atoms from a water molecule and two mono-μ-oxo groups. The coordination mode of the terpy ligand is meridional as observed in all Mn complexes containing this ligand.[19−29,31] The Mn−OH_2 distance (2.023(6) Å) is close to those observed in the complexes **2**[15] and **3**[16] (average 2.045 and 2.009 Å, respectively). This distance is also significantly longer than the Mn^{IV}−OH bond distance of 1.830 Å in **4**[17] confirming that the bound species is an aqua group. Each coordination sphere of Mn(2) and Mn(3) consists of the central nitrogen and the two distal oxygen atoms of the $terpyO_2$ ligands, and three oxygen atoms of μ-oxo bridges. A point of interest is that the seven-membered chelate rings of $terpyO_2$ produce a flexible structure that contains the ligand in a facial coordination mode rather than the meridional arrangement typical for the parent terpy ligand. This facial coordination induces significant ligand strain with the result that the three pyridyl rings of the $terpyO_2$ are not coplanar.

The central pyridine ring lies at an angle of approximately 30° to the mean planes of the two other pyridine N-oxide moieties. The average of the Mn−O bond lengths for the pyridine N-oxide is 1.975 Å. Note that, these structural features are unique in the literature since no other manganese complex with such ligands has yet been crystallized. In fact, there are only a few studies that report coordination complexes of polypyridinyl N-oxide ligands with first row transition metals.[32−34,56] The complexes isolated with Fe, Co, Ni, and Cu are always at the +II oxidation state[56] while with Mn, both +II and

Table 1. Selected Bond Distances (Å) and Angles (deg) for **5**

Mn(2)−O(4)	1.807(5)	Mn(3)−O(3)	1.818(5)
Mn(2)−O(1)	1.808(5)	Mn(3)−O(1)	1.813(5)
Mn(2)−O(2)	1.815(5)	Mn(3)−O(2)	1.818(5)
Mn(2)−O(5)	1.967(5)	Mn(3)−O(7)	1.980(5)
Mn(2)−O(6)	1.969(5)	Mn(3)−O(8)	1.984(5)
Mn(2)−N(4)	2.065(6)	Mn(3)−N(7)	2.074(7)
Mn(1)−O(3)	1.761(5)	Mn(1)−N(1)	1.990(6)
Mn(1)−O(4)	1.761(5)	Mn(1)−N(2)	2.012(6)
Mn(1)−O(9)	2.023(6)	Mn(1)−N(3)	2.005(6)
Mn(1)−Mn(2)	3.2230(18)	Mn(2)−Mn(3)	2.6772(17)
Mn(1)−Mn(3)	3.242(18)		
Mn(1)−O(3)−Mn(3)	129.9(3)	Mn(2)−O(1)−Mn(3)	95.3(2)
Mn(1)−O(4)−Mn(2)	129.2(3)	Mn(2)−O(2)−Mn(3)	94.9(2)
O(4)−Mn(2)−O(1)	98.1(2)	O(1)−Mn(3)−O(2)	83.2(2)
O(4)−Mn(2)−O(2)	97.0(2)	O(1)−Mn(3)−O(3)	96.1(2)
O(1)−Mn(2)−O(2)	83.4(2)	O(2)−Mn(3)−O(3)	97.1(2)
O(4)−Mn(2)−O(5)	87.2(2)	O(1)−Mn(3)−O(7)	171.7(2)
O(1)−Mn(2)−O(5)	174.4(2)	O(2)−Mn(3)−O(7)	92.1(2)
O(2)−Mn(2)−O(5)	94.3(2)	O(3)−Mn(3)−O(7)	91.3(2)
O(4)−Mn(2)−O(6)	90.1(2)	O(1)−Mn(3)−O(8)	93.1(2)
O(1)−Mn(2)−O(6)	92.7(2)	O(2)−Mn(3)−O(8)	172.1(2)
O(2)−Mn(2)−O(6)	172.3(2)	O(3)−Mn(3)−O(8)	90.2(2)
O(5)−Mn(2)−O(6)	89.1(2)	O(7)−Mn(3)−O(8)	90.7(2)
O(4)−Mn(2)−N(4)	165.5(2)	O(1)−Mn(3)−N(7)	92.1(3)
O(1)−Mn(2)−N(4)	94.1(2)	O(2)−Mn(3)−N(7)	91.9(3)
O(2)−Mn(2)−N(4)	92.2(2)	O(3)−Mn(3)−N(7)	168.5(2)
O(5)−Mn(2)−N(4)	80.9(2)	O(7)−Mn(3)−N(7)	81.2(3)
O(6)−Mn(2)−N(4)	81.4(2)	O(8)−Mn(3)−N(7)	81.2(3)
O(3)−Mn(1)−O(4)	100.1(2)	N(1)−Mn(1)−N(2)	79.3(2)
O(3)−Mn(1)−N(1)	175.2(2)	N(3)−Mn(1)−N(2)	158.2(3)
O(4)−Mn(1)−N(1)	84.7(2)	O(3)−Mn(1)−O(9)	86.8(2)
O(3)−Mn(1)−N(3)	100.9(2)	O(4)−Mn(1)−O(9)	173.0(3)
O(4)−Mn(1)−N(3)	89.0(2)	N(1)−Mn(1)−O(9)	88.4(3)
N(1)−Mn(1)−N(3)	79.1(3)	N(3)−Mn(1)−O(9)	89.7(2)
O(3)−Mn(1)−N(2)	100.3(2)	N(2)−Mn(1)−O(9)	86.9(2)
O(4)−Mn(1)−N(2)	91.8(2)		

(56) Amoroso, A. J.; Burrows, M. W.; Dickinson, A. A.; Jones, C.; Willock, D. J.; Wong, W.-T. *J. Chem. Soc., Dalton Trans.* **2001**, 225–227.

Table 2. Distances (A) and Angles (deg) of the $\{Mn_3O_4\}^{4+}$ Core in Complexes **1**−**5** and Reported Exchange Coupling Constants[a]

	1	**2**	**3**	**4**	**5**
Mn(1)−Mn(2,3)$_{av}$[b]	3.243	3.256	3.249	3.184	3.233
Mn(2)−Mn(3)	2.682	2.679	2.675	2.595	2.678
Mn(1)−O(4,3)$_{av}$[c]	1.763	1.766	1.765	1.797	1.761
Mn(2,3)−O(4,3)$_{av}$[d]	1.833	1.842	1.814	1.804	1.813
Mn(2,3)−O(1,2)$_{av}$[e]	1.820	1.806	1.807	1.814	1.814
Mn(1)−O(4,3)−Mn(2,3)$_{av}$[f]	128.83	128.98	130.40	124.35	129.54
O(3)−Mn(1)−O(4)	101.04	100.72	98.77	97.76	100.14
Mn(2)−O(1,2)−Mn(3)$_{av}$[g]	94.43	95.74	95.50	91.36	94.64
Mn(2)−O(1)−O(2)−Mn(3)	163.6	163.9	161.6	161.4	161.8
(Mn(2),Mn(3),O(4),O(3))/ (Mn(1),O(4),O(3))	0	0	0	26.6	0
J_a (cm^{-1})	−54	−49	n.d.	−11	−37
J_b (cm^{-1})	−85	−91	n.d.	−76	−53
reference	14	15	16	17	this work

[a] For clarity, the atom numbering used for **5** has been employed for **1**−**4**. [b] Average distance between the Mn(1)−Mn(2) and Mn(1)−Mn(3) bonds. [c] Average distance between the Mn(1)−O(4) and Mn(1)−O(3) bonds. [d] Average distance between the Mn(2)−O(4) and Mn(3)−O(3) bonds. [e] Average distance between the Mn(2)−O(1), Mn(2)−O(2), Mn(3)−O(1) and Mn(3)−O(2) bonds. [f] Average angle between Mn(1)−O(4)−Mn(2) and Mn(1)−O(3)−Mn(3). [g] Average angle between Mn(2)−O(1)−Mn(3) and Mn(2)−O(2)−Mn(3).

+III oxidation states are found in $[Mn(bpyO_2)_3]^{3+}$ (bpyO_2 = 2,2′-bipyridine 1,1′-dioxide), $[Mn(terpyO_3)_2]^{2+/3+}$ (terpyO_3 = 2,2′:6′,2″-terpyridine 1,1′,1″-trioxide)[32,33] and $[Mn(terpyO_2)_2]^{2+}$.[34] In addition, facial coordination has only been evidenced in the structurally characterized $[Ni(terpyO_3)_2]^{2+}$ complex while in $[M(terpyO_2)_2]^{2+}$ ones (M = Ni, Fe) a meridional arrangement is observed.[34,56]

Finally, the coordination of two terpyO_2 ligands to the basal Mn ions (Mn(2) and Mn(3)) in **5** leads to an environment richer in oxygen atoms compared to **1**−**3** which, surprisingly, does not affect the structural geometry of the $\{Mn_2(\mu\text{-}O)_2\}$ unit. The relationship between core structural parameters and magnetic properties is discussed below.

EPR and Magnetic Properties. In general, a multicenter magnetically coupled system is viewed as consisting of N spin sites interacting through $N(N-1)/2$ Heisenberg exchange couplings J_{ij}, and is described by the isotropic Heisenberg−Dirac−van Vleck Hamiltonian:[57−60]

$$H_{\text{eff}} = -2\sum_{i<j} J_{ij}\hat{S}_i\cdot\hat{S}_j \qquad (1)$$

where $\hat{S}_i$ is the spin operator of the ith metal center. For **5**, the number of possible pairwise exchange couplings is three. By assuming that the two mono-μ-oxo bridges are equivalent, eq 1 results in the simplified Hamiltonian eq 2 which takes into account only two distinct magnetic interactions.[61]

$$H_{eff} = -2J_a(\hat{S}_1\hat{S}_2+\hat{S}_1\hat{S}_3) - 2J_b\hat{S}_2\hat{S}_3 \qquad (2)$$

where J_a represents the interaction parameter of the two exchange paths featuring the mono-μ- oxo bridges and J_b refers to the exchange path characterized by a bis-μ-oxo bridge (Figure 2). Using the Kambe vector coupling model,[62] the spin operators $\hat{S}_A = \hat{S}_2 + \hat{S}_3$ and $\hat{S}_T = \hat{S}_1 + \hat{S}_A$ can be introduced in eq 2, leading to the energies of the spin levels given in eq 3 that depend only on the values of the intermediate spin S_A and the total spin S_T.[63]

$$E(S_T, S_A) = -(J_b - J_a)S_A(S_A+1) - J_aS_T(S_T+1) \qquad (3)$$

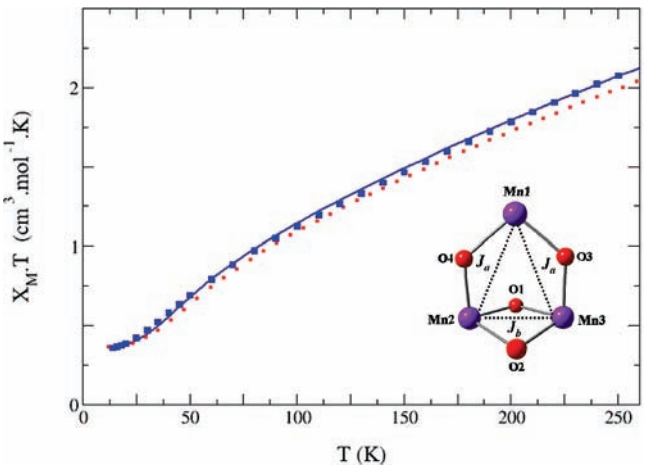

Figure 2. Plot of the $\chi_M T$ product per mole of **5** vs temperature. The solid line (blue) corresponds to a fit of the experimental data (blue square) with $g = 1.98$ (fixed value), $J_a = -37\ cm^{-1}$, $J_b = -53\ cm^{-1}$. The dotted line (red) has been calculated using the theoretical values $J_a = -39.4\ cm^{-1}$, $J_b = -53.0\ cm^{-1}$, $g = 1.98$. Inset: schematic view of complex **5** with the possible magnetic pathways.

Variable temperature magnetic susceptibility measurements were carried out on a powder sample of **5**. The product of the molar magnetic susceptibility (χ_M) and the temperature (T) as a function T is provided in Figure 2. At 300 K, the $\chi_M T$ product of 2.35 $cm^3\ mol^{-1}$ K is far above 1.75 $cm^3\ mol^{-1}$ K, approximate value measured on complexes **1**−**3**. We thus can anticipate a weaker magnetically coupled system in **5**. The $\chi_M T$ product measured at room temperature is also far below the 5.63 $cm^3\ mol^{-1}$ K value expected for three uncoupled Mn^{IV} ions with an electronic spin of $S = 3/2$. The magnetic behavior of **5** indicates a moderate antiferromagnetic coupling between the electronic spins of the three metallic ions leading to a

(57) Dirac, P. A. M. *Proc. Roy. Soc.* **1929**, *A123*, 714.
(58) Heisenberg, W. *Z. Physik* **1926**, *38*, 411–426.
(59) Heisenberg, W. *Z. Physik* **1928**, *49*, 619–636.
(60) Van Vleck, J. H. In *The Theory of Electronic and Magnetic Susceptibilies*; Oxford University: London: 1932; p 384.
(61) Martin, R. L. *New Pathways in Inorganic Chemistry*; Cambridge University Press: New York, 1968.
(62) Kambe, K. *J. Phys. Soc. Jpn.* **1950**, *5*, 48–51.
(63) Kahn, O. *Molecular magnetism*; VCH: New York, 1993.

Scheme 2

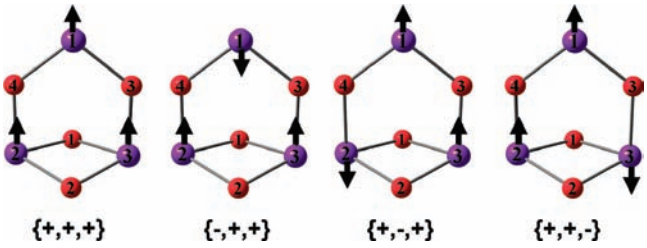

spin $S = 1/2$ ground state, fully in agreement with the $\chi_M T$ value measured at low temperature (0.35 cm^3 mol^{-1} K at 10 K). Using the energies given in eq 3,[63] a good fit was found with $J_a = -37$ (± 0.5) cm^{-1}, $J_b = -53$ (± 1) cm^{-1} and with a fixed g value of 1.98 (Figure 2). The doublet ground spin state is confirmed by powder EPR spectroscopy with a unique isotropic signal centered at a g value just below 2 at low temperature (Supporting Information, Figure S1).

Theoretical Calculations. a. Methodological details. Complex **5** consists of three magnetically interacting manganese(IV) centers and can be described reasonably well by the BS-DFT approach,[35,36,39] as already demonstrated in studies of related systems.[44,64,65] The predicted number of possible pairwise exchange couplings is three and can be determined within the BS-DFT framework. For that purpose, we first assume that locally all spins on each given fragment are aligned in parallel (local HS configurations). Then a separate solution for each of the possible spin configurations of the cluster is computed where each center assumes either a positive or a negative sign of the local spin (denoted as "spin-up" and "spin-down", respectively). Assuming a non-symmetrical structure, a $S = 9/2$ HS configuration {+,+,+} and three $M_S = 3/2$ {−,+,+}, {+,−,+} and {+,+,−} BS solutions can be generated (Scheme 2). Since the trinuclear cluster in question has C_2 point-group symmetry as depicted in Scheme 2 (the C_2 axis passing through Mn(1) and the center of the diamond core unit formed by Mn(2), Mn(3), O(1), and O(2)), the {+,+,−} spin configuration will not be further considered in our analysis, the {+,−,+} and {+,+,−} solutions being equivalent by symmetry. This is fully consistent with the proposed coupling scheme (see eq 2).

From the calculated energies of the HS configuration ($E_{\{+,+,+\}}$) and the two BS states ($E_{\{-,+,+\}}$) and ($E_{\{+,-,+\}}$) (see Supporting Information), the J values of **5** are obtained from the use of eq 2 as

$$J_a = -\frac{(E_{\{+,+,+\}} - E_{\{-,+,+\}})}{18}$$
$$J_b = -\left[\frac{(E_{\{+,+,+\}} - E_{\{+,-,+\}})}{9} + J_a\right] \quad (4)$$

Based on the computed coupling constants, the full magnetic sublevel spectrum can be determined according to eq 3, especially the low energy spin levels.

(64) Sinnecker, S.; Neese, F.; Lubitz, W. *J. Biol. Inorg. Chem.* **2005**, *10*, 231–238.
(65) Sinnecker, S.; Neese, F.; Noodleman, L.; Lubitz, W. *J. Am. Chem. Soc.* **2004**, *126*, 2613–2622.

Table 3. Calculated and Experimental Exchange Coupling Constants J (cm^{-1}) for **5**, Spin of Ground (S_{GS}) and First Excited (S_{ES}) States, and Energetic Separation between the Ground and the Lowest Excited States ($\Delta E_{(GS\text{-}ES)}$) in cm^{-1}

	J_a (cm^{-1})	J_b (cm^{-1})	S_{GS}	S_{ES}[a]	$\Delta E_{(GS\text{-}ES)}$ (cm^{-1})
calc.	−39.4	−55.9	(1/2, 1)	(1/2, 2)	66.0
				(3/2, 0)	85.2
				(3/2, 1)	118.2
				(3/2, 2)	184.2
				(3/2, 3)	283.2
exp.	−37 (±0.5)	−53.0 (±1)	(1/2, 1)	(1/2, 2)	64
				(3/2, 0)	79
				(3/2, 1)	111
				(3/2, 2)	175
				(3/2, 3)	271

[a] (S_T,S_A) with S_T the total spin of the complex and S_A the intermediate spin resulting from the coupling of the manganese ions coordinated by a bis-μ-oxo bridge.

b. Heisenberg Exchange Coupling Constants. In a previous study on magnetic properties of polynuclear manganese clusters,[44] it was shown that the problem of deriving a set of J−values might be underdetermined. Specifically, the number of experimentally probed energy levels (typically two or three) might be not large enough to ensure that the fitting procedure leads to a unique set of J-values. Thus, the simultaneous study of the magnetic sublevel spectrum and of the resulting magnetic susceptibility is advocated as the most reliable way to compare theory and experiment.

In this context, the calculated J-values based on the BS-DFT approach of **5** are collected in Table 3 together with the relevant energy spectrum calculated by a direct diagonalization of the Heisenberg Hamiltonian. In Table 3, we also indicate the total spin of the ground and the lowest excited states, as well as the energetic separation between the ground and these lowest spin multiplets. The full energy spectra of the spin states of **5** and the corresponding Boltzmann populations are provided in the Supporting Information, Table S3 and Figure S2.

Looking first at the J values presented in Table 3, our results already provide excellent agreement with the experimental data. The computed coupling constants both reflect moderate antiferromagnetic interactions as expected from experiment and from the results of most of the studies reported on manganese clusters since the two exchange paths are here mediated by μ-oxo bridges.[5,6] From the computed magnetic sublevel spectrum, we confirm that both ground and first excited spin states are doublet $S_T = 1/2$ states and that their energetic separation very closely matches the value probed by experiment. The same observations can be also made for the next excited levels with all features being assigned to quartet ($S_T = 3/2$) states. Moreover, from the Boltzmann population analysis, we observe that only the first five levels are significantly populated (above 10%) within the range of experimental temperatures (see Supporting Information, Figure S2). We can thus confirm that the spin states reported in Table 3 are the only relevant states for the present study of complex **5**.

Furthermore, one more step toward observable quantities was taken: in Figure 2 the magnetic susceptibility curve ($\chi_M T$ vs T) constructed from the theoretical results[55] are compared with the data deduced from

Scheme 3. Schematic Representations of **4** and **5** (purple, Mn; red, O; blue, N)[a]

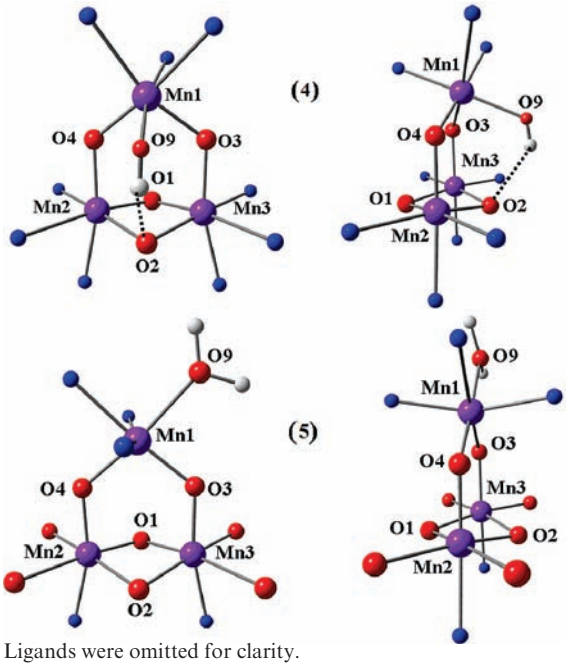

[a] Ligands were omitted for clarity.

experiment. These graphical results are in line with the analysis of the data presented in Table 3 and show the nice correlation between theory and experiment for the prediction of magnetic properties of **5**.

In addition, it is interesting to analyze the ground spin state of this system in terms of magneto-structural correlations. In former experimental studies on $\{Mn_3O_4\}^{4+}$ clusters,[14,15,17] it was actually suggested that their ground spin state could be correlated to the magnitude of the J parameters that are directly influenced by specific geometrical features. For the case of **1**−**2**,[14,15] the ground spin state was found to be $S_T = 1/2$ and the magnetic susceptibility fit parameters were $J_a = -54$ and $J_b = -85$ cm^{-1} as well as $J_a = -49$ and $J_b = -91$ cm^{-1}, respectively. However, very different results were obtained with **4**:[17] the ground spin state was $S_T = 3/2$ and the derived J parameters were $J_a = -11$ and $J_b = -76$ cm^{-1}. The principal origin of the spin-state change in going from a doublet to a quartet appeared to be the magnitude of the J_a coupling constant which is 5-fold smaller for **4** whereas the J_b parameter remains almost constant when compared to **1** and **2**. The decrease in J_a was shown to be related to the chemical nature of the first coordination sphere of the Mn(1) center, that is, N_4O_2 for **1** and **2** and N_3O_3 for **4**. In **4**, an OH ligand is coordinating the Mn(1) site which leads to a pulling of Mn(1) toward O(2) and presumably to the formation of a hydrogen bond between O(2) and O(9). This hydrogen bond appears to be partly responsible for a specific distortion resulting in a dihedral angle between the planes defined by Mn(2), Mn(3), O(3), O(4) on one hand and Mn(1), O(3), O(4) on the other (Scheme 3).[17] For **1** and **2**, no distortion is observed so that the Mn(1) center rests in the O(4), Mn(2), Mn(3), O(3) plane. Upon looking at **5**, the aqua ligand coordinated to Mn(1) is in *trans* position versus the mono-μ-oxo bridge O(4) contrarily to the *cis* coordination of the hydroxo ligand in **4** versus the two mono-μ-oxo bridges O(3) and O(4). This is imposed by the meridional coordination of terpy in contrast to the facial coordination of bpea. This peculiar position of the aqua ligand prevents the bending observed in **4** and leads to the planar structure of the $\{Mn_3O_4\}^{4+}$ core as for **1** and **2**.

Since the above geometrical features were found to be responsible for the relative magnitudes of the J_a and J_b parameters, they also modulate the ratio J_a/J_b that controls the nature of the ground spin state.[10,11,66] Indeed, for $J_a/J_b = 0.4$, the $S_T = 1/2$ and $S_T = 3/2$ states are degenerate. Thus, for $1 \geq J_a/J_b \geq 0.4$, the $S_T = 1/2$ state ($S_A = 1$) is the ground spin state of the system, while for $0 \leq J_a/J_b \leq 0.4$, it is the $S_T = 3/2$ state ($S_A = 0$).[17] The above observation can be verified for complexes **1**−**2** and **4**−**5** since for **1**−**2** and **5**, characterized by a doublet ground state, it was found that $0.54 \leq J_a/J_b \leq 0.70$, while for **4**, the quartet ground state is associated to $J_a/J_b = 0.14$.

Concerning the magnitude of the exchange coupling constants of **5**, J_a and J_b, they are noticeably smaller than those found for **1** and **2**. This is particularly astonishing since the structural features of the $\{Mn_3O_4\}^{4+}$ core of **5** are similar to those of complexes **1** and **2** (Table 2). Intuitively, comparable magnetic properties for these three complexes might have been expected. Indeed, it is generally admitted that for the oxo bridged manganese dinuclear units, correlations can be found between the structural and the magnetic properties of the $\{Mn_2(\mu\text{-}O)_x\}^n$ core ($x = 1-3$, n depends on the oxidation state of the Mn ion),[65,67−69] as in the case of $\{Mn^{IV}{}_2(\mu\text{-}O)_2\}^{4+}$, for which a correlation has been found between the J values and the Mn−O−Mn angle.[70] By contrast, our results demonstrate that, in the peculiar trinuclear $\{Mn^{IV}{}_3O_4\}^{4+}$ core, the magnitude of the exchange couplings does not depend exclusively on the structure of the core, but the ancillary ligands might also play a crucial role. The presence of additional oxygen ligands may lead to a modification of the electronic structure within the manganese cluster and thus a decrease in J values.

Conclusions

In summary, we have obtained a new example of a trinuclear oxo bridged Mn cluster featuring a triangular $\{Mn^{IV}{}_3O_4\}^{4+}$ core. The X-ray structure has been resolved, and the magnetic properties were investigated through a combination of experimental techniques and quantum chemistry. Interestingly, this complex represents the first structurally characterized Mn compound with polypyridinyl N-oxide ligands. Looking at the magnetic properties of **5**, the quantum chemical analysis of the trinuclear unit, based on the TPSSh functional, provides an excellent match with the experimental data. Further work is in progress in our

(66) McCusker, J. K.; Jang, H. G.; Wang, S.; Christou, G.; Hendrickson, D. N. *Inorg. Chem.* **1992**, *31*, 1874–1880.
(67) Barone, V.; Bencini, A.; Gatteschi, D.; Totti, F. *Chem.—Eur. J.* **2002**, *8*, 5019–5027.
(68) Rudberg, E.; Salek, P.; Rinkevicius, Z.; Agren, H. *J. Chem. Theory Comput.* **2006**, *2*, 981–989.
(69) Stamatatos, T. C.; Christou, G. *Phil. Trans. R. Soc. A* **2008**, *366*, 113–125.
(70) Law, N. A.; Kampf, J. W.; Pecoraro, V. L. *Inorg. Chim. Acta* **2000**, *297*, 252–264.

laboratories to elucidate the role of the nature of the ancillary ligands on exchange interactions between the Mn ions in determining the ground state total spin of this and closely related systems.

Acknowledgment. This work was supported by the bilateral France−New Zealand Actions Intégrées Program (Dumont d'Urville 2006-2007) and France−Germany Hubert Curien Program-DAAD (Procope 2008-2009). F.N. gratefully acknowledges financial support from the DFG priority program 1137 "Molecular Magnetism", from the University of Bonn and from the Max Planck Society. The authors thank Dr. C. Philouze (DCM, Université Joseph Fourier de Grenoble) for preliminary crystallographic measurements and Dr. J.-M. Latour (CEA-Grenoble) for preliminary magnetic measurements on the complex.

Supporting Information Available: Relationship between the exchange coupling constants and the energies of the spin configurations, crystallographic data for **5** (Table S1), powder Q-band EPR spectrum of **5** (Figure S1), calculated energies and energetic separations between the HS and BS states (Table S2), calculated energy spectra of the spin states of **5** (Table S3) and calculated Boltzmann populations of **5** (Figure S2). Crystallographic data in CIF format. This material is available free of charge via the Internet at http://pubs.acs.org. CCDC 740778 contains the supplementary crystallographic data for **5**·3.54H_2O. These data can be obtained free of charge from the Cambridge Crystallographic Data Center via www.ccdc.cam.ac.uk/data_request/cif.